



# Presence of boulders associated with an extreme wave event in the western Mediterranean (Cape Cope, Murcia, Spain): possible evidence of a tsunami

Javier Lario<sup>1</sup>  · Chris Spencer<sup>2</sup> · Teresa Bardaji<sup>3</sup> 

Received: 26 September 2022 / Accepted: 1 March 2023 / Published online: 20 March 2023  
© The Author(s) 2023

## Abstract

The region of Murcia, in the southeast of the Iberian Peninsula, experiences moderate tectonic activity, with earthquakes of up to 6.2–6.9 Mw recorded. Even with seismic activity of this scale there is no geological or instrumental record of tsunamis affecting the area. The presence at Cape Cope, Murcia of a ridge of metre-sized imbricated boulders (comprised of Upper Pleistocene sediments) reaching a height of up to 4 m above sea level, indicates that there has been an extreme wave event in the area during the Holocene. Through studying the wave conditions generated during large storms in this area, the boulder ridges appear to have been caused by extreme waves associated with a seismic event, as a tsunami.

**Keywords** Extreme wave event · Boulders transport · Tsunami · Geological record

## Presencia de bloques asociados a un evento de oleaje extremo en el Mediterráneo occidental (Cabo Cope, Murcia, España): posible evidencia de un tsunami

### Resumen

La región de Murcia, en el sureste de la Península Ibérica, registra una actividad tectónica moderada, registrándose terremotos de hasta 6,2-6,9 Mw. Aún con una actividad sísmica de esta magnitud no existen registros geológicos ni instrumentales de tsunamis que hayan afectado a la zona. La presencia en Cabo Cope, Murcia, de un cordón litoral de bloques imbricados de tamaño métrico (compuestos por rocas del Pleistoceno superior) que alcanzan una altura de hasta 4 m sobre el nivel del mar, indica que en la zona se ha producido un evento de oleaje extremo durante el Holoceno. Mediante el estudio de las condiciones de oleaje generadas durante grandes tormentas en esta zona, se infiere que este cordón litoral de bloques parece haber sido causado por oleaje extremo asociado a un evento sísmico, como un tsunami.

**Palabras clave** Evento de oleaje extremo · Transporte de bloques · Tsunami · Registro geológico

## 1 Introduction

The processes resulting in the deposition of coarse-clast ridges in coastal settings has been discussed in recent years. Scheffers et al. (2009) in their studies of storm/tsunami deposits in the Caribbean listed the main diagnostic features discriminating between storm-induced and tsunamigenic coarse deposits and concluded that boulder rampart/ridges formed by tsunami include: boulders of over 300 tons; megaclasts diminishing in size landward; a seaward strip of bare rock; imbrication strongly present; the presence of seaward slopes and smooth landward slopes or boulders being mostly

---

✉ Javier Lario  
javier.lario@ccia.uned.es

<sup>1</sup> Facultad de Ciencias, Universidad Nacional de Educación a Distancia (UNED), Madrid, Spain

<sup>2</sup> Faculty of Environment and Technology, UWE Bristol, Bristol, UK

<sup>3</sup> Facultad de Ciencias, Universidad de Alcalá, Alcalá de Henares-Madrid, Spain

angular. Some studies (Noormets et al., 2004; Nott, 2004; Scheffers, 2005) have shown that extreme storm waves are not as efficient as tsunamis in the detachment of, and transport of large boulders. Mastronuzzi et al., (2007a, 2007b) argued that the use of boulder accumulations as indicators of tsunamis has been a matter of debate as boulder accumulations can also result from storm wave action. Noormets et al. (2004) indicated that tsunamis, as well as large swell waves, are capable of quarrying large boulders, provided that enough initial fracturing is present.

Spike and Baldburgh (2011) reviewed published examples of boulder transport by tsunamis and concluded that various criteria, for example, the size and mass of boulders, as well as the distance of the boulder deposits to the coast and their position above sea-level, were frequently used to discriminate between a tsunami or storm origin (Bryant & Nott, 2001; Mastronuzzi & Sansò, 2000; Scheffers et al., 2009; Whelan & Kelletat, 2005) and that boulders entrained and transported by tsunamis were supposed to have larger sizes and greater mass, and should be transported further inland than storm boulders (Goto et al., 2009; Whelan & Kelletat, 2005).

Scheffers and Kinis (2014) described multiple imbricated boulder deposits (most of them as ramparts or ridges) with storm or tsunami origins. They completed a comprehensive review of existing literature and concluded that all of these imbricated boulder deposits were associated with tsunamis. They also concluded that generally, strong imbrication, even in large boulders (from 10 to > 200 tons in weight), is best developed in coarse tsunami deposits.

Etienne et al. (2011) argued that there are no published accounts of extensive boulder ridge formations by tsunami in any case studies of recent events, but some authors have described boulder trains originated by the 2004 Indian Ocean tsunami (Goto et al., 2007; Nandasena et al., 2011b; Paris et al., 2009). Yamanda et al. (2014) described concentrations of boulders (instead of ridges or alignments) in three major clusters, in relation to the 2011 Tohoku-oki tsunami at Miyako City, Japan. Also, Goto et al. (2012) described boulder deposits that originated from the same tsunami. Recently Lau et al. (2018) identified lines of large coral reef boulders in Fiji, associated with a 1953 tsunami.

Spike and Bahlburg (2011) found that if the different waves of a tsunami wave train had sufficient energy to entrain clasts, the transport would occur step by step in a landward direction. The process of entrainment, transport, and deposition will be repeated two or three times thus building the groups which then give the appearance of a single transport sequence. The proposed multi-step process model has also been reported in other tsunami boulder transport studies (Nandasena et al., 2011b). Cox et al. (2019) reported wave-tank experiments testing whether storm events could generate imbricated boulder ridges and they found that storm

waves can produce all of the features of imbricated boulder deposits and concluded that these types of deposits cannot be used as de facto tsunami indicators. Therefore, the discussion about the origin of boulder ridges due to extreme wave events is still open and a range of approaches and interpretations exist in the literature.

De Martini et al. (2021) founded the Mediterranean area as an ideal open laboratory for paleotsunami research for multiple reasons and conclude that the area appears to be ideal also to face the problematic storm vs. tsunami source differentiation that is very critical in the reconstruction of a paleotsunami history at a specific site. The presence along the Mediterranean coast of large boulders was firstly reported in Greece by Pirazzoli et al (1999). Other studies have described boulders accumulations in several sites of the long coastal perimeter of the Mediterranean (i.e.: 2019a; Alvarez-Gómez et al., 2011; Barbano et al., 2010; Kelletat & Schellmann, 2002; Lario et al., 2017; Maouche et al., 2009; Mastronuzzi & Sansò, 2000, 2004; Mastronuzzi & Pignatelli, 2006; Mastronuzzi et al., 2007a, 2007b; Roig-Munar et al., 2018a; Scheffers et al., 2008; Scicchitano et al., 2012; Shah-Hosseini et al., 2013; Vött et al., 2008, 2019).

Tsunami generation models show that in the Iberian Peninsula, Murcia is the province affected by the greatest tsunamis, mainly generated by large seismic events in Northern Algeria. The Balearic Islands Ibiza and Minorca also recorded the highest maximum elevations, with heights that may pass the four-meters mark locally. (Alvarez-Gómez et al., 2011).

In the Mediterranean Spanish Coast has been described scarce geological records of EWE (Extreme Wave Events) such as tsunamis or storm surges. Even some historical tsunamis have been reported in the region, their impact at the coast was negligible (De Martini et al., 2021). During the past years some boulders deposits, usually with ridge morphology, have been studied in the area.

Roig-Munar et al. (2019a) founded large boulders on marine cliffs in more than 20 study sites on Majorca Island. Deposits consist of large imbricated boulders of up to 25 t located on platforms that form the rocky coastline of the island, several tens of meters from the edge of the cliff, up to 15 m above sea level. They are mainly located on the eastern and southern coasts of Majorca, where wave height and energy are low compared with those from the N and NE. The study conclude that a tsunami appears to be a more likely mechanism for transportation and deposition of the boulder field than storm waves. Along the rocky coastline of Minorca Island circa 25 sites with large imbricated boulders deposits have been found on platforms located several tens of meters from the edge of the cliff, up to 15 m above the sea level (Gomez-Pujol & Roig-Munar, 2013; Martín-Prieto et al., 2019; Roig-Munar et al., 2018a). Roig-Munar et al. (2018a) analysed 3000 large boulders along the studied

sites and concluded that they should be dislodged and positioned by the action of tsunami waves, although some of these boulders were also displaced by storm waves. Also, in seven study sites on Ibiza and Formentera Islands large boulder deposits were located several tens of meters from the edge of the cliff, up to 11 m above sea level and several kilometers away from any inland escarpment (Roig-Munar et al., 2019b). Six sites were identified in North Castellon, Valencia Region with boulders ridges with sedimentary characteristics typical of tsunamis flows (Roig-Munar et al., 2018b). In 1522 there was an earthquake  $M > 6.5$  in Almería that affected large areas of the western Mediterranean. The epicentral area is located offshore on the platform of the Gulf of Almería. The earthquake triggered several underwater landslides that could have produced a tsunami (Reicherter & Becker-Heidmann, 2009). Tomassetti et al. (2021) described in Malaga a tsunami deposit in an archaeological context assigning it to an earthquake documented in historical sources in the year 881 AD.

The study of the boulder ridge located at Cope Cape complements the studies carried out so far and confirms the occurrence of tsunamis in eastern Spanish coast.

## 2 Geological and climatic setting

### 2.1 Geodynamical framework

The structural framework of the eastern Betic Cordilleras (SE Spain) is linked to the occurrence of a large left-lateral transcurrent zone known as the Eastern Betics Shear Zone (EBSZ) (Larouzière et al., 1988; Silva et al., 1993) that evolved since the middle Miocene because of the continuous northward indentation of the Aguilas Arc block (Coppier et al., 1989). The Aguilas Arc is a differentially up-thrusted cortical structure characterized by a large-scale bending driven by two main fault systems— $N10^{\circ}$ – $20^{\circ}$  E system (Palomares—Los Arejos faults) and  $N90^{\circ}$ – $100^{\circ}$  E (El Saladillo—Las Moreras faults) that separates the arc

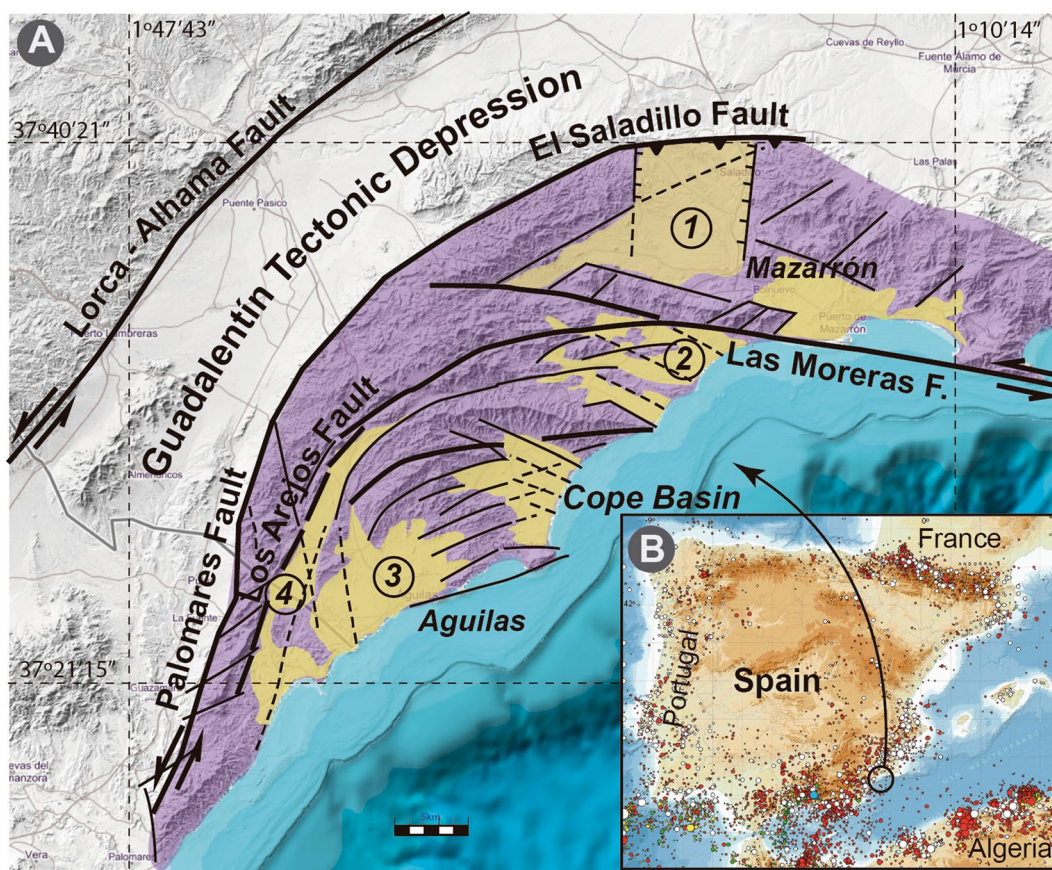


**Fig. 1** **A** Location of the studied area (Cope Basin) within the structural framework of the Aguilas Arc. Main ranges of the Aguilas Arc shaded in violet; Neogene-Quaternary sedimentary basins in light orange (1. Mazarrón Basin; 2. Ramonete Basin; 3. Aguilas Basin; 4. Los Arejos Corridor); **B** Seismic activity in the Iberian Peninsula and

north Africa (IGN). White circles—historical earthquakes. Depth of instrumental earthquakes—red circles (0–30 km); yellow circles (30–60 km); green circles (60–180 km); blue circles ( $\geq 600$  km). Diameter of circles is related to the magnitude of recorded events, with maximum instrumental magnitude never exceeding  $M7.5$

itself from the Guadalentín Tectonic Depression, what in fact is the central segment of the EBSZ (Silva et al., 1993) (Fig. 1). Repeated rotation of the regional stress field from N–S to NNW–SSE since Tortonian times (Coppier et al., 1989; Grievaud, 1989; Montecat et al., 1987; Ott d'Estevou & Montecat, 1985; Silva et al., 1993) promoted the opening of different sedimentary basins within the Aguilas Arc (Fig. 1), that have evolved differentially depending on their location within the arc and on the direction and kinematics of their inner faults (Bardají, 1999). Cope Basin has been defined as a littoral detachment basin (Bardají, 1999) given its extensional behaviour within the general compressive tectonic framework. N120° E and N60° E faults drove its opening during the early Pliocene and later evolution of this basin (Fig. 1A).

The Eastern Betics Shear Zone is one of the most seismically active areas of the Iberian Peninsula (Fig. 1b), however most of this activity is concentrated in the periphery of the Aguilas Arc, along those fault systems oriented perpendicularly or slightly oblique to the main stress field. The strongest earthquakes, reaching magnitude 5.2 Mw (instrumental) or 6.2 to 6.9 Mw (estimated magnitude for historical earthquakes; Alfaro et al., 2012; Martínez Díaz et al., 2011) are associated to these ENE–WSW to E–W faults (e.g. Lorca—Alhama and Bajo Segura faults) that outline the periphery of the Arc. Other active faults that run in parallel to the main N–S trending stress field, such as the Palomares fault system (N10°–20° E) yield very high slip rates (30 km lateral offset since the early Pleistocene; Bousquet, 1979; Weijermars, 1987) but very low seismic activity ( $\leq 3$ Mw) even along its N120° E prolongation (Saladillo fault). In the Aguilas Arc itself, the main master faults show high displacement rates but scant seismic activity (minimal instrumental earthquakes  $\leq 4$ Mw; and only two historic earthquakes reported in Aguilas (AD1596 and AD1882) with maximum MSK intensity of IV–V (Mezcua, 1982). Liquefaction structures and shoreline vertical displacements have been identified in the Cope Basin (Bardají et al., 2015) and related to seismic activity during MIS 5e—Holocene. Both features point to a maximum seismic intensity between VII and IX, after the INQUA ESI-07 macroseismic scale (Environmental Seismic Intensity Scale; Guerreri & Vittori, 2007).

Regarding to submarine faults that could act as a potential tsunamigenic source, no one has been reported close to the studied area but mainly in the Alboran Sea where the 2016 earthquake (Mw 6.4) is the largest ever recorded event. Main active faults capable of generate tsunamis in the southern Iberian coasts are the Al-Idrissi, the Serrata–Carboneras and the Yusuf–Habibas fault zones (Gràcia et al., 2019; Somoza et al., 2021; Vázquez et al., 2021, and references there in).

## 2.2 Sedimentary filling of the Aguilas basin

The studied boulder deposits are located in the Aguilas basin. The earliest sedimentary filling of this basin was strongly dominated by Plio-Pleistocene fossiliferous yellow marine calcarenites, the extension and outcrop of which are controlled by the above mentioned N60° E and N120° E faults (Fig. 2). This unit is unconformably overlain by a well-cemented, sea-level-controlled, off-lapping Pleistocene sedimentary sequence, gently descending to the sea, where coastal gravel sediments alternate with subaerial alluvial fans (Bardají, 1999; Bardají et al., 1986, 2015; Dabrio et al., 1991; García-Tortosa et al., 2004; Zazo et al., 2013). The whole sequence is composed of up to ten marine units, with the three more recent ones presenting a staircase arrangement within the general off-lapping trend. These three younger units have been attributed to MIS7, MIS 5e and MIS 5 c/a based on the faunal content (*Strombus bubonius*) and specific lithology (oolithic dune-beach associated to the intermediate unit) (Bardají et al., 2009, 2015). The younger of these three units (quartzous beach-dune system) is scarcely represented along the basin but the two older ones are widely developed along the coast usually recorded on top of a wave-cut platform carved into the lower yellow calcarenites (Fig. 3).

MIS7 unit (B in Fig. 3) is characterised by fine bedded (decimetre scale) calcarenites alternating with gravel layers, deposited in a foreshore-shoreface environment. MIS5 unit (D in Fig. 3) is a grey conglomerate of coastal origin, characterized by abundant white rounded quartz pebbles, cobbles and some boulders. Occasionally along the shore, reddish terrestrial sediments separate this unit from the older one (Unit C in Fig. 3) (Bardají et al., 2015).

In the studied zone (shaded in grey in Fig. 2), these units are eroded by the present-day wave-cut platform where the extreme wave event (EWE) displaced boulders are located, the provenance and source lithology of which are the MIS7 and MIS5 units (described above) as well as the underlying yellow calcarenites.

## 2.3 Meteorological conditions

Due to its latitude and location in the southeast of the Iberian Peninsula, the location is affected by very diverse atmospheric conditions, associated with the interaction of cold polar and warm tropical air masses. During much of the year it is subjected to the action of aerological shelter exerted by the Azores anticyclone that is responsible for long and intense droughts. However, the characteristics of the weather and, above all, the production of rain, depends more closely on polar mechanisms than on tropical ones (Capel Molina, 1991). Although the territory of Murcia is outside the area of greatest turbulence and cyclogenesis, located to the north

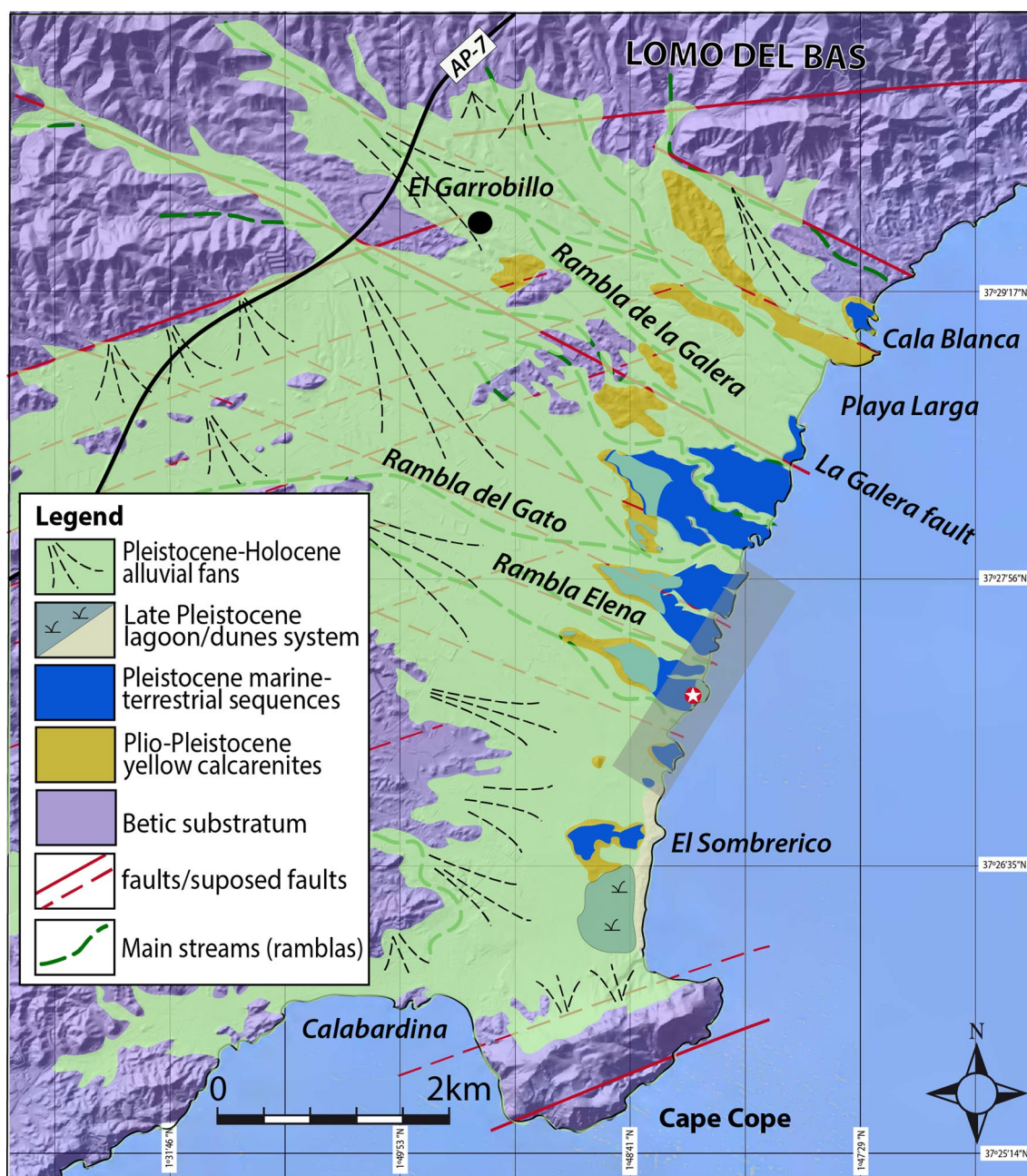


**Fig. 2** Geological scheme showing the main geological units of Cope Basin (Bardají, 1999) The 'studied zone' is shaded in grey, and white star in red circle mark the location of boulder ridge outcrop studied in detail in this work (Figs. 4 and 5)

of the 40° parallel, it remains under the influence of meridian circulation flows from the east, isolated cold irruptions in height (vortices detached from the jetstream) and thermoconvective processes developed in the western Mediterranean that trigger significant torrential rain events (Conesa & Alonso, 2006).

The presence of storms in the Mediterranean associated with convection phenomena gives rise to a regime of easterly winds (*levantes*), typically humid on the eastern flank of the region and drying out as they move inland. This situation predominates during spring and summer, extending until autumn. The frequency distribution of the wind directions in the Murcia region varies according to the geographical

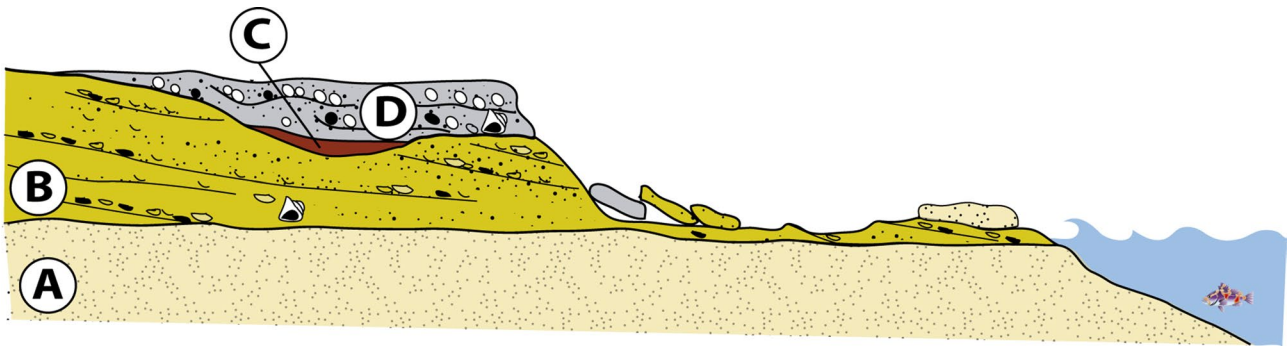


**Fig. 3** Schematic sequence of sedimentary units outcropping in the studied zone. **A** Plio-Pleistocene yellow calcarenites; **B** MIS7 fine bedded beach unit; **C** intermediate terrestrial sediments; **D** MIS5 quartzous gravel beach

situation and the topographic relief of the area. Although the winds of the first quadrant dominate in a large part of the region, it is in the eastern coastal zone where they are more persistent, especially in summer, with observed frequencies of 26.5% for the E direction, 29.6% for the winds from the NE and 16% for those from the SE. In winter, on the other hand, winds from the north are more frequent: NW 19.2% and N 15.8% (Conesa & Alonso, 2006).

Since there are no oceanographic parameter buoys around Cape Cope, SIMAR (operational wave prediction system) data was used to establish the maritime climate ([\[osdeleestado.es\]\(http://osdeleestado.es\)\). The SIMAR dataset consists of time series data \(in this case covering the period 1958–2021\) of wind and wave parameters from numerical modelling. The source is therefore synthetic data and does not come from direct measurements. This study utilised SIMAR point 2,067,089, the nearest to the study area \(5.5 km east of Cape Cope\). Maximum monthly significant wave heights \( \$H\_s\$ \) at this point during 1958–2022 period have been calculated as 2.23–4.27 m at this point. At the SIMAR point the significant swell recorded resulted mainly from the E \(50% of the time\) and from the SSW \(28% of the time\).](http://www.puert</a></p>
</div>
<div data-bbox=)

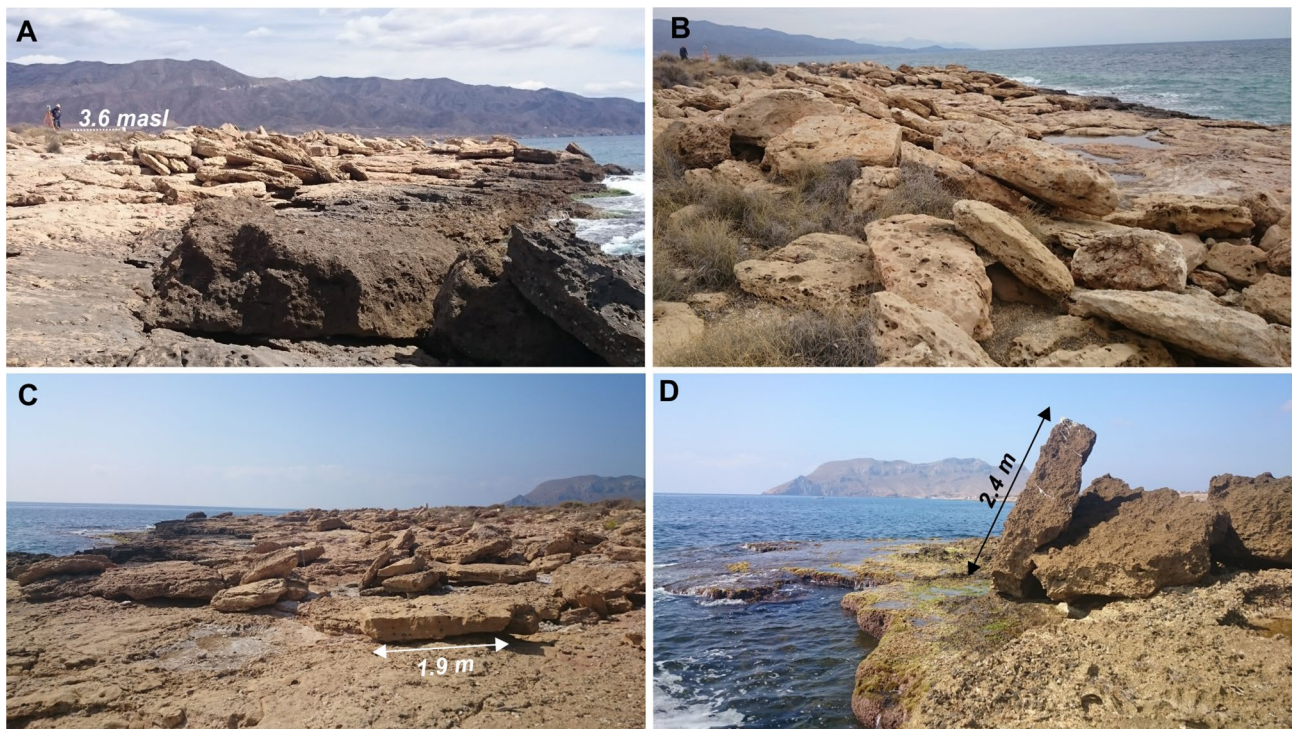


**Fig. 4** **A** Imbricated boulder ridge on top of the Late Pleistocene marine platform. **B** Detail of imbricated boulders. **C** Isolated and imbricated boulders. **D** > 2 m long turned boulder

For a real maximum wave height that has been recorded from direct measurement, data from the nearest sea buoy, Cabo de Palos (code 1613), located 75 km NE of Cabo Cope, has been utilised. During the period 1985–2012 the measured monthly maximum heights varied between 5.66 m and 14.8 m, and the significant heights ( $H_s$ ) between 2.94 m and 5.64 m.

### 3 Boulder accumulation of Cape Cope

Deposits consisting of heterometric boulders were recorded along the coast to the north of Cape Cope (Fig. 2). The boulders formed a ridge parallel to the coastline, but also isolated boulders were present in the study area. The main boulder ridge reached heights of 4.0 m asl and were composed largely of angular boulders, but also with some sub-rounded and rounded boulders present. Some boulders appeared to be imbricated and some individual boulders had long axes of  $> 4.15$  m, volumes of up to  $7.1 \text{ m}^3$  and weights of 17.7 tonnes (Fig. 4).

The boulders under investigation in this study were made up of three different lithologies (Bardají et al., 2015): (1) Yellow fossiliferous calcarenites of medium-coarse grain size and massive character (Upper Pliocene–Lower Pleistocene); (2) Calcarenites of medium-fine grain size alternating with layers of gravels of variable thickness, and layers with frequent bivalve molds (Upper Pleistocene); (3) Highly cemented grey conglomerates in which two facies have been differentiated, a conglomerate of very rounded gravels (1–2 cm) mainly of white quartz, and a heterometric conglomerate with very rounded gravels, pebbles, and boulders of different lithologies (Upper Pleistocene). Three younger units present a staircase arrangement in the general offlapping sequence with the youngest further staircased into the two older units. The youngest was only barely visible in a single outcrop at 0.5 m asl but the two older ones were easy to trace along the basin and have been attributed to MIS 7 and MIS 5 (Bardají et al., 2009, 2015). The boulder deposits appeared to originate from joint bounded blocks (JBB) originally forming part of a wave-cut platform carved into the Plio-Pleistocene and the Upper Pleistocene marine terraces.

For the geolocation of the boulder ridges, several flights were made with a DJI Phantom 4 unmanned aerial vehicle (drone), that carried out a photogrammetric flight and subsequent 3D modelling utilising Pix4D software. To obtain a centimetric resolution of the geolocation of the boulders and their dimensions, various control points were obtained with a Trimble Rover R8 GNSS GPS system. To obtain millimetric detail, terrestrial photogrammetry of the boulders was carried out using the commercial software Agisoft Metashape. Three-dimensional restitution and modelling of the boulders and integrating the resulting products of both

the photogrammetric flight and the terrestrial photogrammetry was completed using GIS facilitated through the free software QGIS (Fig. 5). In this way, the morphometry, orientation, altitude, and the distance from the coastline of each boulder was determined.

To calculate the densities of the different lithologies identified, a minimum of 2–3 samples of each was taken. In the laboratory, each was submerged in water for at least 24 h to achieve total saturation to accurately simulate the submerged environment. Once saturated each sample was weighed ( $m_i$ ) and the volume ( $v_i$ ) of each sample was calculated by immersing them in water and measuring the volume of displacement. All measurements were made twice to minimize errors. Finally, the density ( $\rho_i$ ) was calculated using the basic formula  $\rho_i = m_i/v_i$ . Average density has been estimated at  $2.5 \text{ gr/cm}^3$ .

Of the outcrops mentioned in Fig. 2, the central outcrop was selected to measure the boulder parameters (south Rambla Elena, star in Fig. 2). A total of 500 boulders were measured, for each boulder the following parameters were recorded; the major axis (a), the middle axis (b) and the minor axis (c), the distance to the coastline, measured to the high-water mark (d), the height above sea level (h), and the angle of the slope of the surface on which it is located (Table 1). Usually, to calculate volume the formula  $V = a \cdot b \cdot c$  is used. Several authors used automatic volume calculation from scanned boulder images and concluded that scan volume variates between 40–60% of the volume calculated by axis estimation (Engel & May, 2012; Lario et al., 2017, 2020). Thus, a correction factor of 60% was applied to the volume calculated by using the  $V = a \cdot b \cdot c$  formula. 48 boulders were selected as representative, including the heaviest and the lightest, the furthest from the coast and the closest, as well as the highest and the closest to sea level, plus a set of randomly selected boulders (Table 1).

The average distance of the boulder deposits to the coast was 19.4 m (ranging from 0.2–39.5 m), the average altitude was 2.5 m asl (with a range of 0.5–4.0 m asl), average corrected volume was  $1.1 \text{ m}^3$  (ranging from 0.04– $7.1 \text{ m}^3$ ) and the average weight was 2796 kg (range being 95.1–17,754 kg). A first approximation demonstrates that, as would be expected, heavier boulders were distributed nearest to the present coast while the lighter boulders were deposited further inland (Fig. 6).

Likewise altitudinal data showed a similar relationship with heavier boulders present at lower heights above sea level than the lighter ones. (Fig. 7).

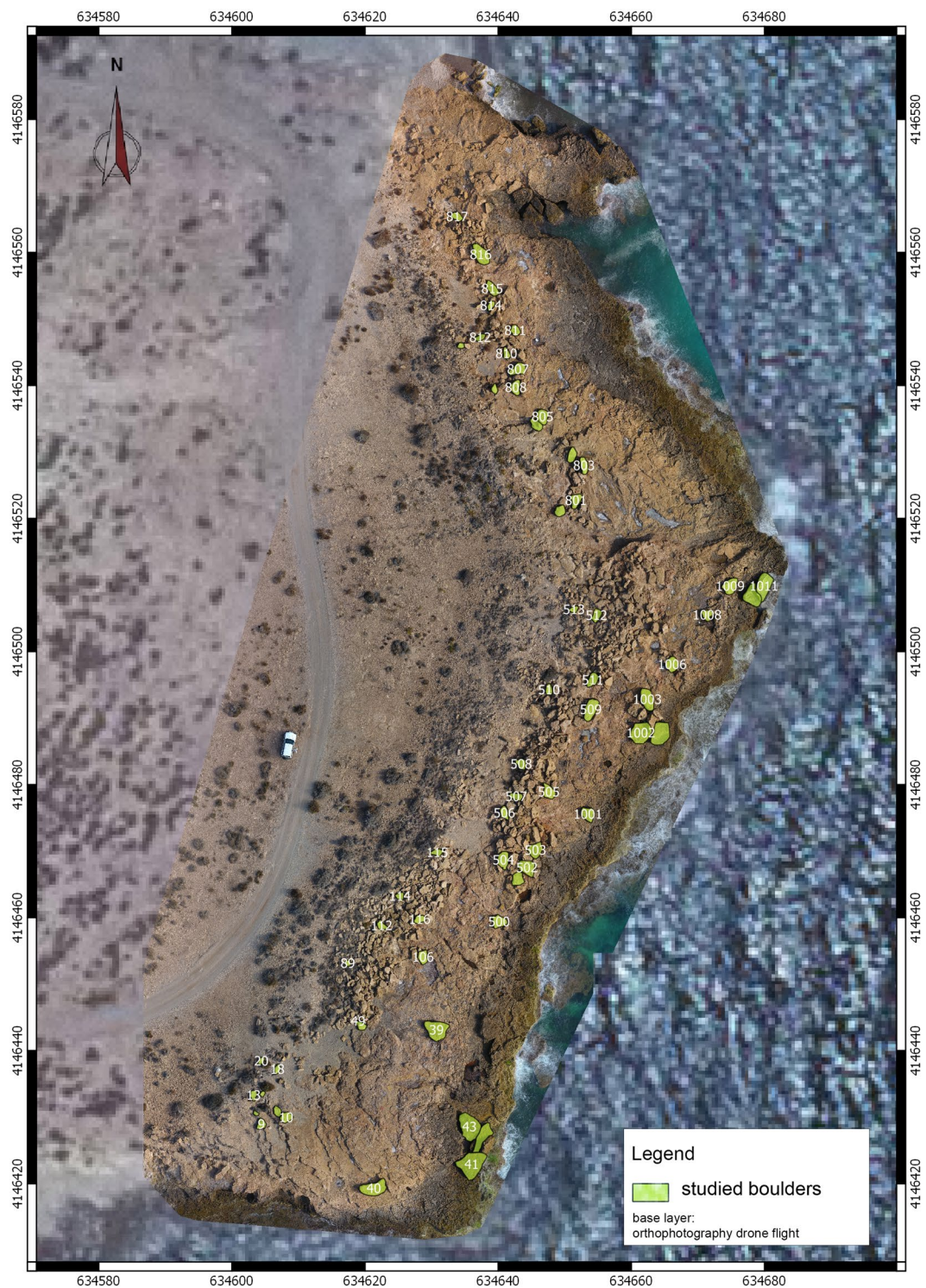


**Fig. 5** Orthophoto obtained by UAV with the location of the studied boulders (central outcrop, south Rambla Elena)



**Table 1** Main parameters of measured boulders

Boulder ID	a	b	c	D	H	CV	Weight kg	JBB Ht	JBB Hs	Sub. Ht	Sub. Hs
CC-816	3.70	2.10	0.45	9.90	2.05	2.11	5268	1.36	5.44	1.66	6.64
CC-1008	1.89	1.68	0.53	7.62	2.62	1.00	2500	1.58	6.31	1.25	5.01
CC-1009	2.63	2.29	0.61	5.80	2.02	2.20	5497	1.82	7.30	1.79	7.14
CC-1011	4.07	2.48	0.90	0.20	0.50	5.48	13,697	2.71	10.86	1.74	6.97
CC-1010	2.69	1.68	1.03	0.50	0.50	2.78	6954	3.08	12.32	0.84	3.36
CC-10	1.66	1.68	0.48	32.81	2.90	0.80	2011	1.45	5.78	1.29	5.14
CC-11	1.71	1.17	0.11	35.52	3.17	0.13	336	0.34	1.35	0.67	2.68
CC-9	0.86	0.53	0.32	36.75	2.98	0.09	216	0.96	3.82	0.27	1.07
CC-12	1.68	1.57	0.48	38.75	3.13	0.75	1883	1.43	5.72	1.18	4.73
CC-14	0.89	0.62	0.17	37.53	3.63	0.06	140	0.51	2.04	0.48	1.91
CC-13	1.51	0.95	0.18	39.48	3.83	0.16	394	0.55	2.21	0.74	2.97
CC-18	1.54	0.83	0.32	35.93	3.62	0.24	612	0.96	3.85	0.56	2.26
CC-40	4.15	1.74	0.92	15.73	1.46	3.99	9972	2.77	11.07	0.97	3.89
CC-39	3.84	3.16	0.57	13.98	2.39	4.13	10,330	1.71	6.83	2.44	9.77
CC-43	4.00	3.22	0.92	6.16	1.07	7.10	17,754	2.77	11.07	2.46	9.85
CC-89	0.75	0.65	0.13	29.21	3.77	0.04	95	0.39	1.56	0.51	2.04
CC-106	2.17	1.42	0.20	17.60	2.58	0.37	920	0.60	2.40	1.01	4.05
CC-112	1.52	1.33	0.38	25.23	3.17	0.46	1149	1.15	4.58	1.01	4.05
CC-114	1.29	1.14	0.25	24.58	3.41	0.22	553	0.75	3.02	0.90	3.60
CC-116	1.81	1.20	0.34	20.09	2.84	0.44	1102	1.01	4.05	0.93	3.71
CC-115	2.11	1.13	0.25	24.82	3.54	0.35	876	0.74	2.95	0.89	3.58
CC-500	2.23	2.17	0.47	7.84	1.68	1.37	3420	1.42	5.66	1.72	6.87
CC-501	1.84	1.77	0.28	10.90	2.17	0.55	1368	0.84	3.37	1.32	5.29
CC-504	2.69	1.57	0.52	15.96	2.40	1.32	3312	1.58	6.30	1.14	4.56
CC-503	2.67	1.52	0.23	12.43	2.22	0.56	1400	0.69	2.77	1.12	4.47
CC-505	2.65	1.72	0.28	13.42	2.18	0.75	1886	0.83	3.32	1.29	5.16
CC-507	2.00	1.09	0.44	18.43	3.10	0.57	1426	1.31	5.24	0.73	2.92
CC-506	1.72	1.12	0.30	19.16	3.59	0.35	867	0.90	3.61	0.87	3.48
CC-508	1.54	1.51	0.36	21.87	3.98	0.50	1256	1.08	4.33	1.19	4.76
CC-509	3.49	1.71	0.39	13.05	2.55	1.41	3513	1.18	4.73	1.35	5.40
CC-511	2.20	1.41	0.49	17.65	2.94	0.91	2280	1.47	5.89	1.01	4.04
CC-1001	2.62	1.83	0.67	6.80	1.52	1.93	4819	2.01	8.06	1.28	5.12
CC-1003	3.60	1.72	0.61	7.21	1.98	2.25	5628	1.82	7.30	1.22	4.88
CC-1006	2.42	2.00	0.31	18.22	2.30	0.90	2248	0.93	3.73	1.48	5.93
CC-800	1.80	1.62	0.42	27.96	2.10	0.74	1841	1.27	5.06	1.26	5.06
CC-801	2.34	1.64	0.35	24.82	2.07	0.81	2030	1.06	4.23	1.30	5.19
CC-803	2.55	1.57	0.40	23.04	1.77	0.96	2388	1.19	4.77	1.23	4.93
CC-804	2.34	0.97	0.47	25.21	2.21	0.64	1600	1.41	5.65	0.58	2.31
CC-805	2.34	1.85	0.16	17.55	2.03	0.42	1053	0.49	1.95	1.00	3.99
CC-809	1.56	0.97	0.23	22.24	3.10	0.21	516	0.69	2.75	0.76	3.05
CC-807	2.46	1.71	0.51	21.40	2.17	1.28	3205	1.53	6.12	1.29	5.16
CC-815	2.60	1.24	0.31	14.06	2.71	0.60	1491	0.93	3.72	0.97	3.89
CC-814	1.58	0.81	0.17	15.21	2.80	0.13	330	0.52	2.08	0.64	2.54
CC-811	1.69	1.40	0.28	15.80	2.16	0.40	997	0.84	3.38	1.10	4.40
CC-812	1.70	0.89	0.26	19.42	3.05	0.24	595	0.79	3.15	0.68	2.71
CC-810	1.82	1.06	0.19	19.43	2.26	0.22	550	0.57	2.28	0.82	3.28
CC-817	1.78	1.16	0.31	15.07	2.60	0.38	960	0.93	3.73	0.90	3.61
CC-513	1.47	1.02	0.45	28.09	3.52	0.41	1013	1.35	5.41	0.65	2.59

*a*, *b*, *c* main axes, *D* distance to coastline (mean sea level), *H* height from coastline (mean sea level), *CV* corrected volume, *Ht* tsunami wave height, *Hs* storm wave height, *JBB* Joint Bounded Boulders, *Sub* Subaerial boulders (Barbano formula)

**Fig. 6** Relation of boulder coastal distance vs. boulder weight

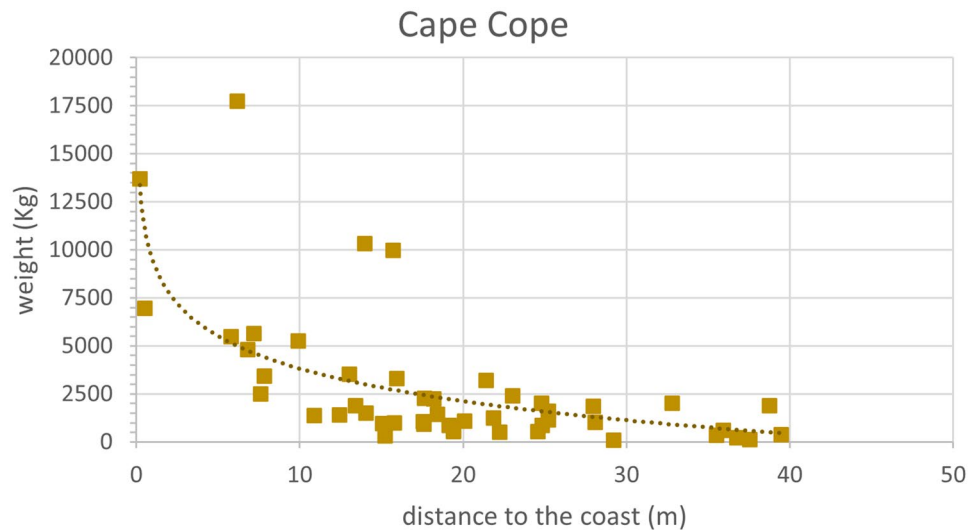
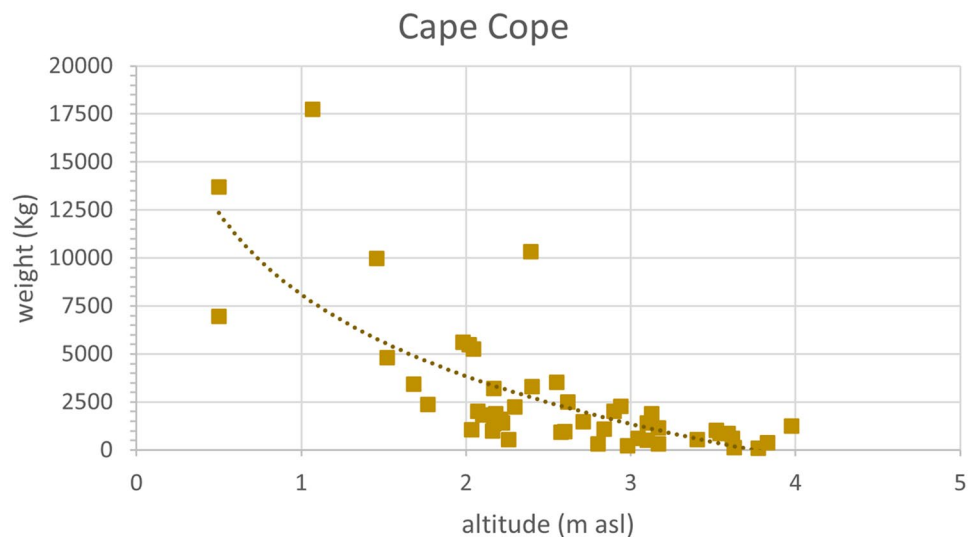


**Fig. 7** Relationship of boulder altitude (m asl) vs. boulder weight



## 4 Estimating extreme wave height, flow velocity and flow depth required to move boulders

### 4.1 Methodology for modelling boulder transport

Several studies have tried to infer the height of waves required to transport boulders at the coast. Nott (2003) presented formulas used to calculate wave heights required to move boulders by both tsunami and storm waves in three different pre-transport situations: submerged boulders; sub-aerial boulders; and joint-bounded blocks (JBB). To incorporate the fact that a boulder has one side facing the wave, one top surface, and is limited by four sides. Later Pignatielli et al. (2009) proposed some modifications to Nott's

equations. Also, Barbano et al. (2010) modified these equations after testing wave transport formulas on the coast of Sicily. Nandasena et al. (2011a) improved Nott's equations further and found that the minimum flow velocity, derived from their revised equation, required to initiate the transport of submerged boulders was less than that inferred from Nott's equations.

Assuming wave heights from the initiation-of-motion approach is sometimes considered questionable, although it has been used in previous work. Mastronuzzi et al., (2007a, 2007b) used Nott's (2003) equations for hydrodynamic calculations relating to boulder accumulations in south-eastern Salento (Italy). This methodology has been used to study the movement of boulders related to extreme wave events (Spike et al., 2008, in the Caribbean; Maouche et al., 2009, in

Algeria; Switzer & Burston, 2010, in southeast Australian; Costa et al., 2011, in southern Portugal; Spike & Baldburgh, 2011, in Chile; Engel & May, 2012, in the Caribbean; Lario et al., 2017 in SW Spain and Lario et al., 2020, in Mexico).

Taking all of these formulas into account, and considering that most of the boulders examined in this study corresponded to a JBB scenario, the equations proposed by Engel and May (2012), that used a modification of Nott's equations proposed by Nandasena et al. (2011a) for the JBB scenario have been applied, where:

$$Ht = \frac{(\rho b - \rho w) \cdot V \cdot (\cos\theta + \mu \cdot \sin\theta)}{2 \cdot \rho w \cdot C_L \cdot a \cdot b \cdot q}$$

$$Hs = \frac{(\rho b - \rho w) \cdot V \cdot (\cos\theta + \mu \cdot \sin\theta)}{0.5 \cdot \rho w \cdot C_L \cdot a \cdot b \cdot q}$$

where *Ht* = tsunami wave height; *Hs* = storm wave height; *C<sub>L</sub>* = coefficient of lift (0.178); *a* = A axis of boulder; *ρw* = density of sea water = 1.02 g/ml; *ρb* = boulder density (in this study an average density of 2.5 g/cm<sup>3</sup> was used); *V* = corrected boulder volume; *q* = boulder area coefficient (0.73); *b* = B axis of boulder; *μ* = coefficient of static friction (0.65); *θ* = bed slope angle of the pre-transport setting.

If the initiation of movement of most of the boulders was in subaerial conditions, the Barbano et al. (2010) modification of Nott's equations, the following formulas, was applied:

$$Ht = \frac{\left[ 0.5 \left( \frac{\rho b - \rho w}{\rho w} \right) \cdot b^2 c g - C_m b c^2 \ddot{u} \right]}{g(C_D c^2 + C_L b^2)}$$

$$Hs = \frac{\left[ 2 \left( \frac{\rho b - \rho w}{\rho w} \right) \cdot b^2 c g - 4 C_m b c^2 \ddot{u} \right]}{g(C_D c^2 + C_L b^2)}$$

where *C<sub>d</sub>* the coefficient of drag = 2; *C<sub>m</sub>* the coefficient of mass = 1; *ü* = 1 m/s<sup>2</sup> is the flow acceleration; *g* is the acceleration due to gravity (9.81 m/s<sup>2</sup>).

Nandasena et al. (2011a) developed a “boulder transport histogram” to represent the range of flow velocities that satisfied the requirements for initial transport of a boulder via different modes of transport: sliding, rolling, saltation or lifting. The boulder transport histogram can be used to predict the possible initial transport modes of a dislodged boulder from the flow velocity.

In the case of a submerged or subaerial boulder the following scenarios exist:

Transport initiates with sliding.

$$u^2 \geq \frac{2(\rho b / \rho w - 1) g c (\mu_s \cos\theta + \sin\theta)}{C_d (c/b) + \mu_s C_L}$$

Transport initiates with rolling (overturning).

$$u^2 \geq \frac{2(\rho b / \rho w - 1) g c (\cos\theta + (c/b) \sin\theta)}{C_d (c^2/b^2) + C_L}$$

Transport initiates with saltation.

$$u^2 \geq \frac{2(\rho b / \rho w - 1) g c \cos\theta}{C_L}$$

Or in the case of a joint-bounded boulder where transport only begins with saltation/lifting:

**Fig. 8** Wave height necessary to move the boulders by storms (*Hs*) or by tsunamis (*Ht*) in a subaerial scenario, applying the Barbano (2010) equations

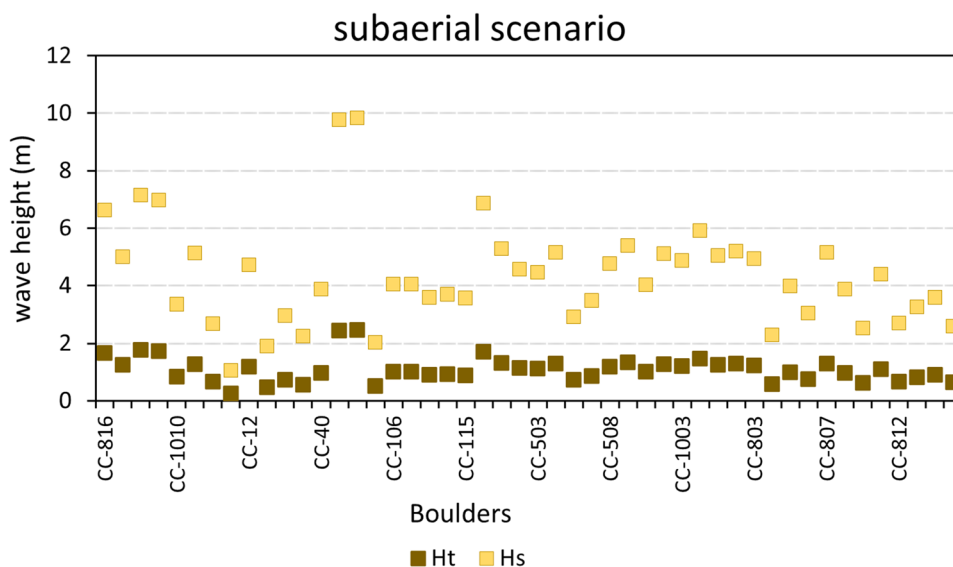
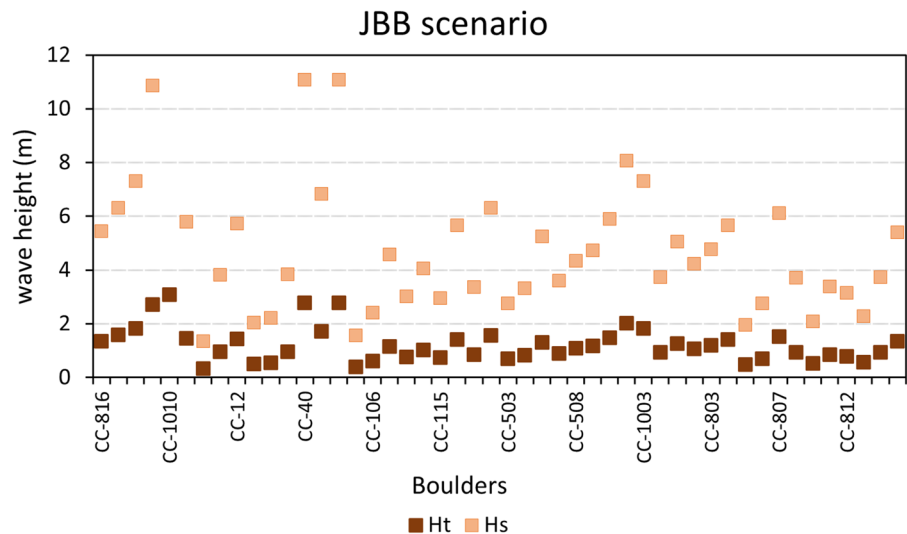


**Fig. 9** Wave height necessary to move the boulders by storms (Hs) or by tsunamis (Ht) in a JBB scenario, applying the Engel and May (2012) equations



$$u^2 \geq \frac{2(\rho_b/\rho_w - 1)gc(\cos\theta + \mu_s \sin\theta)}{C_d}$$

In Eqs. (5) to (8),  $u$  is the flow velocity,  $g$  is gravitational acceleration ( $9.81 \text{ m/s}^2$ ),  $\mu_s$  is the coefficient of static friction between the boulder and the bed (0.7) and  $C_d$  is the coefficient of drag (1.95) (Nandasena et al., 2011a, 2014).

A relationship between flow depth and flow velocity described by the Froude number as  $Fr = u/\sqrt{gh}$ , where  $h$  is the flow depth, was used to estimate the flow departing depth from the minimum flow velocity required to move a boulder (Nandasena et al., 2014). The Froude number for past tsunamis has been determined to be between 0.7 and 2.0; in this study values of 1.0 and 1.5 were used, as proposed by Nandasena et al., (2012, 2014).

## 4.2 Results

The results obtained by applying formulas (3) and (4) to the boulders of the Cabo Cope site are presented in Table 1. They show that to move the heaviest and largest boulders in subaerial conditions, tsunami wave height would need to exceed 1.75 to 2.45 m (based on mass of the five largest boulders found in different locations in the study area). The height of storm waves capable of moving those boulders would need to be at least 6.90 to 9.85 m (Fig. 8).

The results obtained using Engel and May (2012) formula for JBB scenarios (Eqs. (1) and (2)) indicated that to move the heaviest and largest boulders, tsunami wave heights would need to have exceeded 2.7 to 3.1 m (based on the mass of the five largest boulders found in different locations in the study area). The height of storm waves capable of moving the same boulders would have needed to be at least 10.9 to 12.3 m. (Fig. 9).

When considering the flow velocity, the results obtained by applying Eqs. (5) to (8) to the boulders investigated in this study (considering weight, distance to the coast and altitude) are presented in Table 2 and Fig. 10 which shows the corresponding boulder transport histogram. These figures also display the minimum flow velocity and range of flow velocities that would have been required to initiate boulder transport at each site. In the case of submerged/subaerial boulders, the average results indicate that a wave celerity of not less than 3.65 m/s would have been required to transport boulders from their pre-transport location. If the average flow velocity was greater than 3.6 m/s, the boulders would have been transported by sliding. If the average flow velocity was  $> 5.7 \text{ m/s}$ , the boulders would have been transported by rolling; if average flow velocity was  $> 7.8 \text{ m/s}$ , boulder transport would have been via saltation.

In the case of the original position of the boulders being a JBB scenario (Fig. 11), the boulder would remain stable until the average flow velocity for transport by saltation/lifting is higher than 8.0 m/s.

Bosnic et al. (2021) modelled the 1755 Lisbon tsunami in the Algarve to assess tsunami onshore flow characteristics. Results from the inverse model demonstrated tsunami onshore average flow velocities ranged from 7.3 up to 9.3 m/s and forward modelling results show tsunami onshore velocities of 7 m/s. These values are similar to the 5 m/s estimation derived from boulder deposits by the 1755 CE Lisbon tsunami in Costa et al. (2011) and also are comparable to the data of Bujan and Cox (2020) where the average onshore velocity for a 3 m offshore tsunami wave was estimated to be around 5 m/s. Consequently, in this study, it appears that the flow velocities calculated as necessary to move the boulders at Cape Cope are similar to the results of previous tsunami studies.

**Table 2** Flow velocity and flow depth calculated to start the movement of the boulders

Boulder ID	Flow velocity (m/s)				Flow depth (m)							
	Sliding	Rolling	Saltation	Lifting	FR = 1				FR:1.5			
					Sliding	Roll	Salt	Lift	Sliding	Roll	Salt	Lift
CC-816	4.35	6.98	8.48	8.79	1.93	4.97	7.33	7.87	0.86	2.21	3.26	3.50
CC-1008	4.04	6.46	9.14	9.47	1.66	4.25	8.51	9.14	0.74	1.89	3.78	4.06
CC-1009	4.65	7.49	9.83	10.18	2.20	5.72	9.84	10.57	0.98	2.54	4.37	4.70
CC-1011	4.97	7.81	11.98	12.42	2.52	6.21	14.64	15.72	1.12	2.76	6.51	6.99
CC-1010	4.22	5.84	12.77	13.23	1.81	3.48	16.62	17.84	0.80	1.55	7.39	7.93
CC-10	4.01	6.44	8.75	9.06	1.64	4.23	7.80	8.37	0.73	1.88	3.47	3.72
CC-11	2.86	4.04	4.22	4.37	0.84	1.67	1.82	1.95	0.37	0.74	0.81	0.87
CC-9	2.36	3.29	7.11	7.37	0.57	1.10	5.16	5.54	0.25	0.49	2.29	2.46
CC-12	3.89	6.24	8.70	9.02	1.55	3.97	7.72	8.29	0.69	1.76	3.43	3.68
CC-14	2.42	3.90	5.20	5.39	0.60	1.55	2.76	2.96	0.27	0.69	1.23	1.32
CC-13	2.89	4.60	5.41	5.61	0.85	2.15	2.98	3.20	0.38	0.96	1.33	1.42
CC-18	2.88	4.49	7.13	7.39	0.85	2.05	5.19	5.57	0.38	0.91	2.31	2.48
CC-40	4.26	6.17	12.10	12.54	1.85	3.88	14.93	16.03	0.82	1.72	6.64	7.13
CC-39	5.22	8.24	9.50	9.85	2.78	6.93	9.21	9.89	1.23	3.08	4.09	4.39
CC-43	5.54	8.92	12.10	12.54	3.13	8.10	14.93	16.03	1.39	3.60	6.64	7.13
CC-89	2.40	3.83	4.55	4.71	0.59	1.50	2.11	2.26	0.26	0.67	0.94	1.01
CC-106	3.38	5.15	5.64	5.84	1.16	2.70	3.24	3.48	0.52	1.20	1.44	1.55
CC-112	3.56	5.72	7.78	8.07	1.29	3.34	6.18	6.63	0.57	1.48	2.75	2.95
CC-114	3.21	5.16	6.32	6.55	1.05	2.71	4.07	4.37	0.47	1.21	1.81	1.94
CC-116	3.39	5.45	7.32	7.59	1.17	3.03	5.46	5.87	0.52	1.35	2.43	2.61
CC-115	3.20	5.13	6.24	6.47	1.04	2.68	3.97	4.26	0.46	1.19	1.77	1.90
CC-500	4.43	7.11	8.66	8.97	2.00	5.16	7.64	8.20	0.89	2.29	3.39	3.64
CC-501	3.84	5.96	6.67	6.91	1.50	3.62	4.54	4.87	0.67	1.61	2.02	2.17
CC-504	3.92	6.23	9.13	9.46	1.57	3.96	8.50	9.12	0.70	1.76	3.78	4.05
CC-503	3.53	5.45	6.05	6.27	1.27	3.03	3.73	4.00	0.57	1.35	1.66	1.78
CC-505	3.79	5.90	6.63	6.87	1.47	3.55	4.48	4.80	0.65	1.58	1.99	2.14
CC-507	3.32	5.13	8.33	8.63	1.12	2.68	7.07	7.59	0.50	1.19	3.14	3.37
CC-506	3.25	5.24	6.91	7.16	1.08	2.80	4.86	5.22	0.48	1.24	2.16	2.32
CC-508	3.73	6.01	7.57	7.84	1.42	3.69	5.84	6.27	0.63	1.64	2.59	2.79
CC-509	3.95	6.36	7.91	8.19	1.59	4.13	6.37	6.84	0.71	1.84	2.83	3.04
CC-511	3.73	5.90	8.83	9.15	1.42	3.54	7.94	8.53	0.63	1.58	3.53	3.79
CC-1001	4.27	6.70	10.32	10.70	1.86	4.57	10.86	11.66	0.83	2.03	4.83	5.18
CC-1003	4.12	6.50	9.83	10.18	1.73	4.31	9.84	10.57	0.77	1.91	4.37	4.70
CC-1006	4.07	6.30	7.02	7.28	1.69	4.04	5.03	5.40	0.75	1.80	2.23	2.40
CC-800	3.90	6.29	8.18	8.48	1.55	4.03	6.83	7.33	0.69	1.79	3.03	3.26
CC-801	3.85	6.17	7.48	7.75	1.51	3.88	5.71	6.13	0.67	1.73	2.54	2.72
CC-803	3.83	6.18	7.95	8.23	1.50	3.89	6.44	6.91	0.66	1.73	2.86	3.07
CC-804	3.17	4.69	8.65	8.96	1.02	2.24	7.62	8.18	0.45	1.00	3.39	3.64
CC-805	3.54	4.90	5.08	5.26	1.28	2.45	2.63	2.82	0.57	1.09	1.17	1.25
CC-809	2.98	4.81	6.04	6.25	0.91	2.35	3.71	3.99	0.40	1.05	1.65	1.77
CC-807	4.05	6.50	9.00	9.32	1.67	4.31	8.25	8.86	0.74	1.91	3.67	3.94
CC-815	3.39	5.47	7.01	7.26	1.17	3.05	5.01	5.38	0.52	1.36	2.23	2.39
CC-814	2.69	4.32	5.25	5.44	0.74	1.90	2.80	3.01	0.33	0.85	1.25	1.34
CC-811	3.52	5.63	6.69	6.93	1.27	3.23	4.56	4.89	0.56	1.43	2.02	2.17
CC-812	2.93	4.70	6.46	6.69	0.87	2.25	4.25	4.56	0.39	1.00	1.89	2.03
CC-810	3.02	4.77	5.50	5.70	0.93	2.32	3.08	3.31	0.41	1.03	1.37	1.47
CC-817	3.31	5.33	7.02	7.28	1.12	2.90	5.03	5.40	0.50	1.29	2.23	2.40

**Table 2** (continued)

Boulder ID	Flow velocity (m/s)				Flow depth (m)							
	Sliding	Rolling	Saltation	Lifting	FR = 1				FR:1.5			
					Sliding	Roll	Salt	Lift	Sliding	Roll	Salt	Lift
CC-513	3.23	4.90	8.46	8.77	1.07	2.45	7.30	7.83	0.47	1.09	3.24	3.48

*F* Froude number

**Fig. 10** Flow velocity necessary to start the boulders movement and move by sliding, rolling or saltation, under a submerged/subaerial scenario. Movement starts at 3.6 m/s (average)

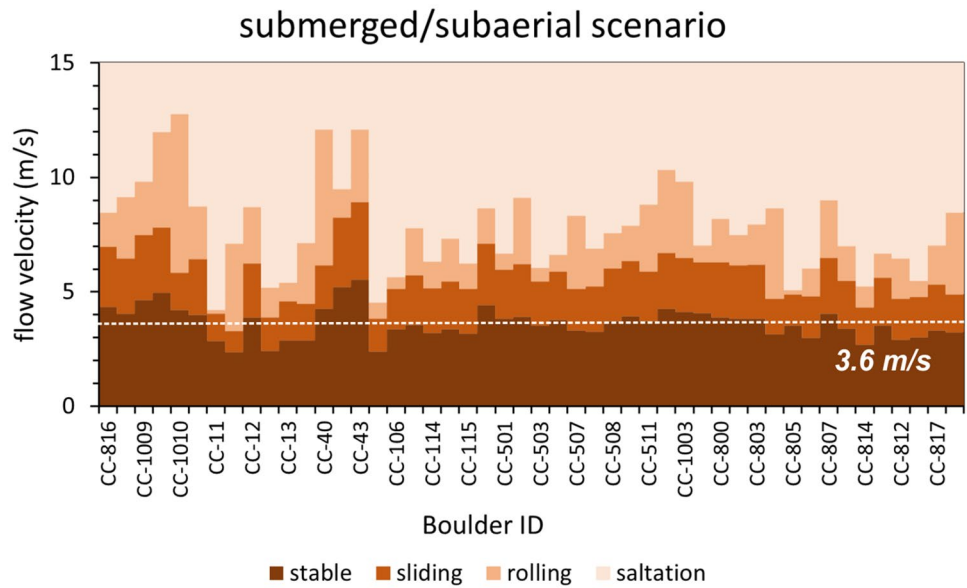


**Fig. 11** Flow velocity necessary to start boulder movement by saltation/lifting, under a JBB scenario. Movement starts at 8.0 m/s (average)

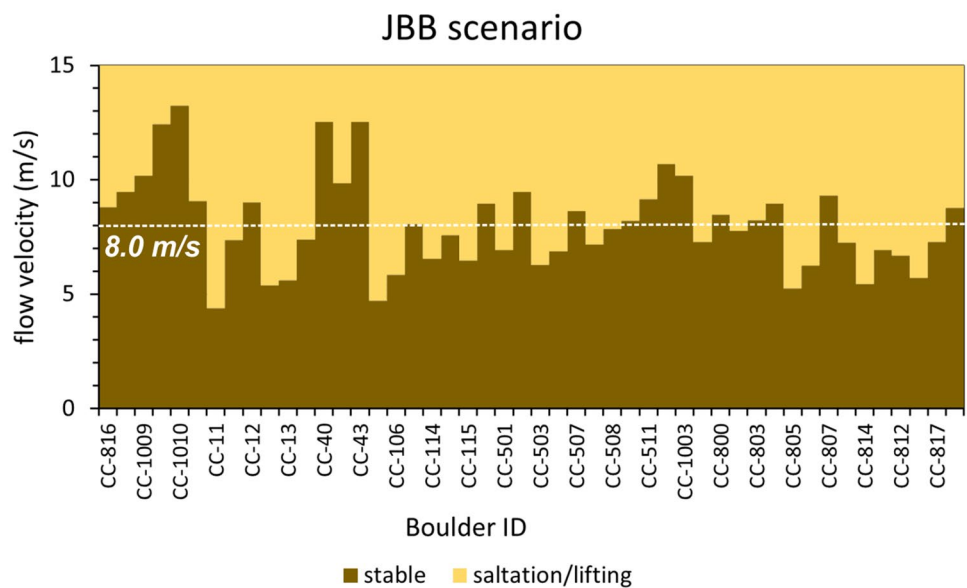


Table 2 presents flow depths necessary to initiate boulder transport using the formulas applied in this paper. Nandasena et al. (2014) indicated the difficulty in establishing the Froude number at each site. Using a  $Fr = 1.0$ , the minimum

flow depth necessary to allow for: (i) sliding averages at 1.4 m; (ii) rolling has an average of 3.5 m; and (iii) for saltation averages at 6.5 m). Lifting, as is the case of JBB, required flow average of 7.0 m. When using  $Fr = 1.5$  the

minimum flow depth for: (i) sliding—average of 0.6 m); (ii) rolling—average of 1.5 m; and (iii) saltation average of 2.9 m. Initiation of boulder movement by lifting requires an average minimum flow of 3.1 m, a value more applicable to the boulder ridges recorded in this study.

## 5 Discussion: extreme event origin and age

The presence of imbricated boulder ridges on the coast of Cape Cope is related to an extreme wave event, either a tsunami or a strong storm. Although there are various formulae relating the deep-water significant wave height to the runup of a wave breaking on the shore that consider seabed topography, wave frequency, or wave amplitude, some approximations from direct measurements suggest a relationship between runup and the significant wave measured offshore (Guza & Thornton, 1982). Senechal et al. (2011) calculated runup from empirical data observed in extreme storm conditions and found that the total vertical runup elevation is significantly correlated to  $H_0$  with this relationship  $R = 2.14 * \tanh(0.4H_0)$ . Thus, the maximum offshore wave heights predicted by the SIMAR network in the area, corresponding to 4.27 m (maximum significant wave height at SIMAR point 2,067,089) and 5.64 m and 14.8 m (maximum significant wave height and maximum wave height at Cabo de Palos buoy). Such waves would have a maximum coastal runup of 2.00 to 2.14 m during extreme storms, far away from the necessary storm waves calculated to move the boulders. It is a fact that the SIMAR record corresponds only to 1951–2021 period, and there may be previous episodes of storms larger than those recorded, although they do not seem to have been observed in the geological record. The necessary waves to move the studied boulders during storms ( $H_s$ ) has been calculated to be between 10.9 to 12.3 m in JBB scenario and between 6.9 to 9.85 m in subaerial setting, therefore, attributing the transport of the boulders to storm events is ruled out utilising the historically recorded extreme sea conditions in this region. Therefore, it is necessary to try to determine whether a possible tsunami could have affected the coast and thus be responsible for this deposit.

In relation to tsunami generation, the decision matrix for tsunamis on the Spanish Mediterranean coast indicates that earthquakes from Mw 6.0–6.5 generated less than 40 km from the coast and at depths of less than 100 km have the potential to generate a destructive tsunami on this coast (IOC, 2011). Tsunami generation models also show that the Murcia region is the area most affected by large tsunamis generated mainly in the north of Algeria (Álvarez-Gómez et al., 2011). Even so, references to tsunamis occurring in the area in historical times are very scarce.

Bardají et al. (2015) reported a tsunami event in Cape Cope occurring during the MIS 5e. In North Castellón (Valencia Region, Spain) six sites were identified with boulder ridges present that have sedimentary characteristics typical of tsunami flows (Roig-Munar et al., 2018, 2019a, 2019b). The boulders had an average weight of 1.5 t and were located at an average distance from the coastline of 15.5 m and at 2.3 m asl. Using the same approaches as used in previous studies the results indicated that local storms were not capable of moving the boulders to their present situation and thus a tsunami wave would appear to be the main cause of transport and deposition. Also, the average boulder orientation indicated that this coastline would be affected by tsunami waves generated in north Algeria passing through the Ibiza-Majorca channel, as has been demonstrated by the models of Alvarez-Gomez et al. (2011). In tsunami catalogues (Lario et al., 2011) there are no data available that provided an age of the events.

Data from Estepona (south Malaga) demonstrates the presence of a sedimentary layer rich in marine and continental materials located at 2.0 m asl, that appears to be representative of a tsunami backwash deposit that is very likely to correspond to the tsunami reported in historical documents that occurred in the 881 AD (Tomassetti et al., 2021).

In 1522, an earthquake of  $M > 6.5$  in Almeria affected large parts of the western Mediterranean, causing more than 1000 deaths. The epicentral area was located on the Gulf of Almeria shelf and produced several submarine landslides that could have produced tsunami (Reicherter & Becker-Heidmann, 2009). These authors found sediments associated with this (and previous) events that indicated wave heights of at least 2–3 m, although evidence of this tsunami has not been found north of Cabo de Gata.

With this context of other tsunami activity in this region the EWE explored in this study can be assigned to a tsunami generated in the western Mediterranean and which may have reached at least 4 m asl on the coast of Cape Cope. Regarding the age of the event, it has not been possible to date the boulders studied but given their disposition with respect to the underlying deposits, their age must be Holocene post-maximum transgressive (ca. 6000 yrBP). The historical earthquakes and tsunamis studied in the area show two possible tsunamis (at 881 AD and 1522 AD) that could be responsible for the boulder ridges present in Cape Cope, although the wave heights referred to in these historical events are far from those necessary to move the boulders. Even in some cases have been possible to suggest a Tsunami Intensity value regard with the environmental impact of the tsunami (Lario et al., 2016), the parameters of the Cope Cape deposits does not allow assigning a scale to the event.

## 6 Conclusions

The characteristics of the deposits found on the coast of Cape Cope conform to the features of an EWE. The application of different equations for the study of wave heights, flow velocity and depth necessary to mobilize these boulders indicate that the extreme storm conditions recorded in the area could not form these boulder ridges, assigning their formation to a high-energy tsunami-type event. These types of deposits are not unique and their presence in other areas of eastern Spain indicates that the occurrence of tsunamis in the area are not isolated events but have occurred on several occasions at least during the Holocene. Once again, the geological record of these events provides data for the study of the seismic hazards on the Mediterranean coast.

**Acknowledgements** This study was funded by the Spanish project CGL2015-69919-R and a grant for the Faculty of Environment and Technology, University of the West of England, Bristol, UK. This work is a contribution to IGCP Project 725 “Forecasting coastal change”, to the INQUA Commission for Coastal and Marine Processes and the Inundation Signatures on Rocky Coastlines (ISROC) Network. Pedro Alfaro and an anonymous reviewer are thanked for their comments.

**Funding** Open Access funding provided thanks to the CRUE-CSIC agreement with Springer Nature. UNED funding for open access publishing.

**Data availability statement** The authors declare that all data supporting the findings of this study are available within the article.

**Open Access** This article is licensed under a Creative Commons Attribution 4.0 International License, which permits use, sharing, adaptation, distribution and reproduction in any medium or format, as long as you give appropriate credit to the original author(s) and the source, provide a link to the Creative Commons licence, and indicate if changes were made. The images or other third party material in this article are included in the article's Creative Commons licence, unless indicated otherwise in a credit line to the material. If material is not included in the article's Creative Commons licence and your intended use is not permitted by statutory regulation or exceeds the permitted use, you will need to obtain permission directly from the copyright holder. To view a copy of this licence, visit <http://creativecommons.org/licenses/by/4.0/>.

## References

- Alfaro, P., Bartolomé, R., Borque, J. M., Estévez, A., García-Mayordomo, J., García-Tortosa, F. J., Gil, A. J., Gràcia, E., Lo Iacono, C., & Perea, H. (2012). The Bajo Segura Fault Zone: Active blind thrusting in the Eastern Betic Cordillera (SE Spain). *Journal of Iberian Geology*, 38(1), 271–284.
- Álvarez-Gómez, J. A., Aniel-Quiroga, I., González, M., & Otero, L. (2011). Tsunami hazard at the Western Mediterranean Spanish coast from seismic sources. *Natural Hazards and Earth System Sciences*, 11, 227–240.
- Barbano, M. S., Pirrota, C., & Gerardi, F. (2010). Large boulders along the south-eastern Ionian coast of Sicily: Storm or tsunami deposits? *Marine Geology*, 275, 140–154.
- Bardají, T. (1999). *Evolución Geomorfológica durante el Cuaternario de las Cuencas Neógenas litorales del Sur de Murcia y Norte de Almería* (p. 492). Universidad Complutense de Madrid.
- Bardají, T., Cabero, A., Lario, J., Zazo, C., Silva, P. G., Goy, J. L., & Dabrio, C. J. (2015). Coseismic vs. climatic factors in the record of relative sea-level changes: An example from the Last Interglacials in SE Spain. *Quaternary Science Reviews*, 113, 60–77.
- Bardají, T., Civis, J., Dabrio, C. J., Goy, J. L., Somoza, L., & Zazo, C. (1986). Geomorfología y estratigrafía de las secuencias marinas y continentales cuaternarias de la Cuenca de Cope (Murcia, España). In F. López & J. B. Thornes (Eds.), *Estudios sobre Geomorfología del Sur de España* (pp. 11–16). Murcia: Universidad de Murcia.
- Bardají, T., Goy, J. L., Zazo, C., Hillaire-Marcel, C., Dabrio, C. J., Cabero, A., Ghaleb, B., Silva, P. G., & Lario, J. (2009). Sea level and climate changes during OIS 5e in the Western Mediterranean. *Geomorphology*, 104, 22–37.
- Bosnic, I., Costa, P. J. M., Dourado, F., La Selle, S. P., & Gelfenbaum, G. (2021). Onshore flow characteristics of the 1755 CE Lisbon tsunami: Linking forward and inverse numerical modelling. *Marine Geology*, 434, 106432.
- Bousquet, P. (1979). Quaternary strike-slip faults in southeastern Spain. *Tectonophysics*, 52, 277–286.
- Bryant, E. A., & Nott, J. (2001). Geological indicators of large tsunami in Australia. *Natural Hazards*, 24, 231–249.
- Bujan, N., & Cox, R. (2020). Maximal heights of nearshore storm waves and resultant onshore flow velocities. *Frontiers in Marine Science*, 7, 309.
- Capel Molina, J. J. (1991). El clima murciano. Dinámica. In A. Morales Gil, & F. Calvo (Eds.), *Atlas de la Región de Murcia*, Presidencia Región de Murcia, La Opinión e Iberdrola. Murcia, 85–96.
- Conesa, C., & Alonso, F. (2006). El clima de la Región de Murcia. In C. Conesa (Ed.), *El Medio Físico de la Región de Murcia* (pp. 95–127). Servicio de Publicaciones.
- Coppier, G., Griveaud, P., Larouziere, F. D., Montecat, C., & Ott d'Estevou, P. (1989). Example of Neogene tectonic indentation in the Eastern Betic Cordilleras: The Arc of Aguilas (Southeastern Spain). *Geodinamica Acta*, 3, 37–51.
- Costa, P. J. M., Andrade, C., Freitas, M. C., Oliveira, M. A., da Silva, C. M., Omira, R., Taborda, R., Baptista, M. A., & Dawson, A. G. (2011). Boulder deposition during major tsunami events. *Earth Surface Processes and Landforms*, 36, 2054–2068.
- Cox, R., O'Boyle, L., & Cytrynbaum, J. (2019). Imbricated coastal boulder deposits are formed by storm waves and can preserve a long-term storminess record. *Scientific Reports*, 9, 10784.
- Dabrio, C. J., Zazo, C., Goy, J. L., Santiesteban, C., Bardají, T., Somoza, L., Baena, J., & Silva, P. G. (1991). Neogene and Quaternary fan-delta deposits in southeastern Spain. *Cuadernos De Geología Iberica*, 15, 327–400.
- De Martini, P. M., Bruins, H. J., Feist, L., Goodman-Tchernov, B. N., Hadler, H., Lario, J., Mastronuzzi, G., Obrocki, L., Pantosti, D., Paris, R., Reicherter, K., Smedile, A., & Vött, A. (2021). The Mediterranean Sea and the Gulf of Cadiz as a natural laboratory for paleotsunami research: Recent advancements. *Earth Science Reviews*, 216, 1–27.
- Engel, M., & May, S. M. (2012). Bonaire's boulder fields revisited: Evidence for Holocene tsunami impact on the Leeward Antilles. *Quaternary Science Reviews*, 54, 126–141.
- Etienne, S., Buckley, M., Paris, R., Nandasena, A. K., Clark, K., Strotz, L., Chagué-Goff, C., Goff, J., & Richmond, B. (2011). The use of boulders for characterising past tsunamis: Lessons from the 2004 Indian Ocean and 2009 South Pacific tsunami. *Earth Science Reviews*, 107, 76–90.



- García-Tortosa, F.J., Leyva, F., & Bardají, T. (2004). Cartografía Geológica y Memoria. *Mapa Geológico de España 1:50.000*, Plan MAGNA, 3ª Serie. Hoja 997 (bis), Cope.
- Gómez-Pujol, L., & Roig-Munar, F. X. (2013). Acumulaciones de grandes bloques en las crestas de los acantilados del sur de Menorca (Illes Balears): Observaciones preliminares. *Geo-Temas*, 14, 71–74.
- Goto, K., Chavanich, S. A., Imamura, F., Kunthasap, P., Matsui, T., Minoura, K., Sugawara, D., & Yanagisawa, H. (2007). Distribution, origin and transport process of boulders deposited by the 2004 Indian Ocean tsunami at Pakarang Cape, Thailand. *Sedimentary Geology*, 202, 821–837.
- Goto, K., Okada, K., & Imanura, F. (2009). Characteristics and hydrodynamics of boulders transported by storm waves at Kudaka Island, Japan. *Marine Geology*, 262, 14–24.
- Goto, K., Sugawara, D., Ikema, S., & Miyagi, T. (2012). Sedimentary processes associated with sand and boulder deposits formed by the 2011 Tohoku-oki tsunami at Sabusawa Island, Japan. *Sedimentary Geology*, 282, 188–198.
- Gràcia, E., Vizcaino, A., Escutia, C., Asioli, A., Rodés, A., Pallás, R., Garcia-Orellana, J., Lebreiro, S., & Goldfinger C. (2010). Holocene earthquake record offshore Portugal (SW Iberia): Testing turbidite palaeoseismology in a slow slow-convergence margin. *Quaternary Science Reviews*, 29, 1156–1172.
- Griveaud, P. (1989). *Etude Géologique du secteur d'Aguilas (Sud-est de l'Espagne): Exemple de poinçonnement néogène dans la zone Bétique interne orientale*. PhD Tesis, Univ. Claude Bernard, Lyon 1, France, 198 pp.
- Guerrieri, L., & Vittori, E. (2007). Environmental Seismic Intensity Scale 2007—ESI 2007. In: *Memorie Descrittive della Carta Geologica d'Italia*, vol. 74. Servizio Geologico d'Italia e Dipartimento Difesa del Suolo, APAT, Roma, Italy, 54 pp.
- Guza, R. T., & Thornton, E. B. (1982). Swash oscillations on a natural beach. *Journal of Geophysical Research*, 87, 483–491.
- IOC (2011). ICG/NEAMTWS: Seventh Session Paris, France 23–25 November 2010. Intergovernmental Oceanographic Commission, Reports of Governing and Major Subsidiary Bodies, p. 45.
- Kelletat, D., & Schellmann, G. (2002). Tsunamis on cyprus: Field evidences and 14C dating results. *Zeitschrift Für Geomorphologie*, 46(1), 19–34.
- Lario, J., Bardají, T., Silva, P. G., Zazo, C., & Goy, J. L. (2016). Improving the coastal record of tsunamis in the ESI-07scale: Tsunami environmental effects scale (TEE-16 scale). *Geologica Acta*, 14, 179–193.
- Lario, J., Spencer, C., Bardaji, T., & Marchante, A. (2017). Eventos de oleaje extremo en la costa del sureste peninsular: Bloques y megabloques como indicadores de tsunamis o tormentas extremas. *Geo-Temas*, 17, 227–230.
- Lario, J., Spencer, C., Bardají, T., Marchante, A., Garduño-Monroy, V. H., Macias, J., & Ortega, S. (2020). An extreme wave event in eastern Yucatán, Mexico: Evidence of a palaeotsunami event during the Mayan times. *Sedimentology*, 67, 1481–1504.
- Lario, J., Zazo, C., Goy, J. L., Silva, P. G., Bardaji, T., Cabero, A., & Dabrio, C. J. (2011). Holocene palaeotsunami catalogue of SW Iberia. *Quaternary International*, 242, 196–200.
- Larouziere, F. D., Bolze, J., Bordet, P., Hernández, J., Montecat, C., & Ott d'Estevou, P. (1988). The Betic segment of the trans-Alboran shear zone during the Late Miocene. *Tectonophysics*, 152, 41–52.
- Lau, A., Terry, J. P., Ziegler, A., Pratap, A., & Harris, D. (2018). Boulder emplacement and remobilisation by cyclone and submarine landslide tsunami waves near Suva City, Fiji. *Sedimentary Geology*, 364, 242–257.
- Maouche, S., Morhange, C., & Meghraoui, M. (2009). Large boulder accumulation on the Algerian coast evidence tsunami events in the western Mediterranean. *Marine Geology*, 262, 96–104.
- Martínez-Díaz, J.J., Rodríguez-Pascua, M.A., Pérez López, R., García Mayordomo, J., Giner Robles, J., Martín-González, F., Rodríguez Peces, M., Álvarez Gómez, J.A., & Insua Arévalo, J.M. (2011). *Informe Geológico Preliminar del Terremoto de Lorca del 11 de mayo del año 2011 (5.1 Mw)*. Instituto Geológico y Minero de España.
- Martin-Prieto, J. A., Roig-Munar, F. X., Rodrigues-Perea, A., & Gelabert, B. (2019). Nova troballa de blocs de tsunami a les costes rocoses de sa Punta de sa Miloca-Corral Fals (Sud de Menorca, illes Balears). *Nemus*, 9, 7–14.
- Mastronuzzi, G., Pignatelli, C., & Sansò, P. (2006). Boulder Fields: A Valuable Morphological Indicator of Paleotsunami in the Mediterranean Sea. *Zeitschrift Für Geomorphologie*, 146, 173–194.
- Mastronuzzi, G., Pignatelli, C., Sansò, P., & Selli, G. (2007a). Boulder accumulations produced by the 20th February 1743 tsunami along the coast of southeastern Salento (Apulia region, Italy). *Marine Geology*, 242, 191–205.
- Mastronuzzi, G., Pignatelli, C., Sansò, P., & Selli, G. (2007b). Boulder accumulations produced by the 20th of February 1743 tsunami along the coast of South Eastern Salento (Apulia region, Italy). *Marine Geology*, 242, 191–205.
- Mastronuzzi, G., & Sansò, P. (2000). Boulders transport by catastrophic waves along the Ionian coast of Apulia (Southern Italy). *Marine Geology*, 170, 93–103.
- Mastronuzzi, G., & Sansò, P. (2004). Large boulder accumulations by extreme waves along the adriatic coast of southern Apulia (Italy). *Quaternary International*, 120, 173–184.
- Mezcu, J. (1982). *Catálogo General de Isosistas de la Península Ibérica*. Instituto Geográfico Nacional. Publicación 202, 319 pp.
- Montecat, C., Ott d'Estevou, P., & Masse, P. (1987). Tectonic-sedimentary characters of the Betic Neogene basins evolving in a crustal transcurrent shear zone (SE Spain). *Bulletin Des Centres De Recherches Exploration - Production Elf-Aquitaine*, 11, 1–22.
- Nandasena, N. A. K., Paris, R., & Tanaka, N. (2011a). Reassessment of hydrodynamic equations: Minimum flow velocity to initiate boulder transport by high energy events (storms, tsunamis). *Marine Geology*, 281, 70–84.
- Nandasena, N. A. K., Paris, R., & Tanaka, N. (2011b). Numerical assessment of boulder transport by the 2004 Indian ocean tsunami in Lhok Nga, West Banda Aceh (Sumatra, Indonesia). *Computers & Geosciences*, 37, 1391–1399.
- Nandasena, N. A. K., Sasaki, Y., & Tanaka, N. (2012). Modelling field observations of the 2011 Great East Japan tsunami: Efficacy of artificial and natural structures on tsunami mitigation. *Coastal Engineering*, 67, 1–13.
- Nandasena, N. A. K., Tanaka, N., Sasaki, Y., & Osada, M. (2014). Reprint of “Boulder transport by the 2011 Great East Japan tsunami: Comprehensive field observations and whither model predictions?” *Marine Geology*, 358, 49–66.
- Noormets, R., Crook, K. A. W., & Felton, E. A. (2004). Sedimentology of rocky shorelines: 3. Hydrodynamics of megaclast emplacement and transport on a shore platform, Oahu. *Hawaii. Sedimentary Geology*, 172, 41–65.
- Nott, J. (2003). Waves, coastal boulder deposits and the importance of the pretransport setting. *Earth Planetary Science Letters*, 210, 269–276.
- Nott, J. (2004). The tsunami hypothesis: Comparisons of the field evidence against the effects, on the Western Australian coast, of some of the most powerful storms on Earth. *Marine Geology*, 208, 1–12.

- Ott d'Estevou, P., & Montenat, C. (1985). Evolution structurale de la zone bétique orientale (Espagne) du Tortonien à l'Holocène. *Comptes Rendus De l'Académie Des Sciences Paris*, 300, 363–368.
- Paris, R., Wassmer, P., Sartohadi, J., Lavigne, F., Barthomeuf, B., Desgages, E., Grancher, D., Baumert, P., Vautier, F., Brunstein, D., & Gomez, C. (2009). Tsunamis as geomorphic crises: Lessons from the December 26, 2004 tsunami in Lhok Nga, west Banda Aceh (Sumatra, Indonesia). *Geomorphology*, 104, 59–72.
- Pignatelli, C., Sanso, P., & Mastronuzzi, G. (2009). Evaluation of tsunami flooding using geomorphologic evidence. *Marine Geology*, 260, 6–18.
- Pirazzoli, P. A., Stiros, S. C., Arnold, M., Laborel, J., & Laborel-Deguen, F. (1999). Late holocene coseismic vertical displacements and tsunami deposits near Kynos, Gulf of Euboea, Central Greece. *Physics and Chemistry of the Earth*, 24, 361–367.
- Reicherter, K., & Becker-Heidmann, P. (2009). Tsunami deposits in the western Mediterranean: Remains of the 1522 Almería earthquake? In K. Reicherter, A. M. Michetti, & P. G. Silva (Eds.), *Palaeoseismology: Historical and Prehistorical Records of Earthquake Ground Effects for Seismic Hazard Assessment* (pp. 217–235). Geological Society.
- Roig-Munar, F. X., Forner, E., Gual, V., Martín-Prieto, J. Á., Segura, J., Rodríguez-Perea, A., Gelabert, B., & Vilaplana, J. M. (2019a). Els blocs de tsunamis de la costa rocosa de la serra d'Irta (el Baix Maestrat): Una proposta com a LIG (Lloc d'Interès Geològic). *Nemus*, 9, 195–210.
- Roig-Munar, F. X., Forner, E., Martín-Prieto, J. Á., Segura, J., Rodríguez-Perea, A., Gelabert, B., & Vilaplana, J. M. (2018b). Presència de blocs de tsunamis i tempestes a les costes rocoses de la serra d'Irta (el Baix Maestrat, País Valencià). *Nemus*, 8, 7–21.
- Roig-Munar, F. X., Rodríguez-Perea, A., Vilaplana, J. M., & Martín-Prieto, J. (2019b). Tsunami boulders in Majorca Island (Balearic Islands, Spain). *Geomorphology*, 334, 76–90.
- Roig-Munar, F. X., Vilaplana, J. M., Rodríguez-Perea, A., Martín-Prieto, J. Á., & Gelabert, B. (2018a). Tsunami boulders on the rocky shores of Minorca (Balearic Islands). *Natural Hazards and Earth System Sciences*, 18, 1985–1998.
- Scheffers, A. (2005). Coastal response to extreme wave events - hurricanes and tsunamis on Bonaire. *Essener Geographische Arbeiten*, 37, 2.
- Scheffers, A., Kelletat, D., Vött, A., May, S., & Scheffers, S. (2008). Late Holocene tsunami traces on the western and southern coastlines of the Peloponnese (Greece). *Earth and Planetary Science Letters*, 269, 271–279.
- Scheffers, A., & Kinis, S. (2014). Stable imbrication and delicate/unstable settings in coastal boulder deposits: Indicators for tsunami dislocation? *Quaternary International*, 332, 73–84.
- Scheffers, S. R., Havisser, J., Browne, T., & Scheffers, A. (2009). Tsunamis, hurricanes, the demise of coral reefs and shifts in prehistoric human populations in the Caribbean. *Quaternary International*, 195, 69–87.
- Scicchitano, G., Pignatelli, C., Spampinato, C. R., Piscitelli, A., Milella, M., Monaco, C., & Mastronuzzi, G. (2012). Terrestrial Laser Scanner techniques in the assessment of tsunami impact on the Maddalena peninsula (South-eastern Sicily, Italy). *Earth, Planets and Space*, 64, 889–903.
- Senéchal, N., Coco, G., Bryan, K. R., & Holman, R. A. (2011). Wave runup during extreme storm conditions. *Journal of Geophysical Research*, 116, C07032.
- Shah-Hosseini, M., Morhange, C., De Marco, A., Wante, J., Anthony, E. J., Sabatier, F., Mastronuzzi, G., Pignatelli, C., & Piscitelli, A. (2013). Coastal boulders in Martigues, French Mediterranean: Evidence for extreme storm waves during the little ice age. *Zeitschrift Für Geomorphologie*, 57(4), 181–199.
- Silva, P. G., Goy, J. L., Somoza, L., Zazo, C., & Bardají, T. (1993). Landscape response to strike-slip faulting linked to collisional settings: Quaternary tectonics and basin formation in the Eastern Betics, southeastern Spain. *Tectonophysics*, 224, 289–303.
- Somoza, L., Medialdea, T., Terrinha, P., Ramos, A., & Vázquez, J. T. (2021). Submarine active faults and Morpho-Tectonics around the Iberian margins: seismic and tsunamis hazards. *Frontiers in Earth Science*, 9, 653639.
- Spiske, M., & Bahlburg, H. (2011). A quasi-experimental setting of coarse clast transport by the 2010 Chile tsunami (Bucalemu, Central Chile). *Marine Geology*, 289, 72–85.
- Spiske, M., Böröcz, Z., & Bahlburg, H. (2008). The role of porosity in discriminating between tsunami and hurricane emplacement of boulders—A case study from the Lesser Antilles, southern Caribbean. *Earth and Planetary Science Letters*, 268, 384–396.
- Switzer, A. D., & Burston, J. M. (2010). Competing mechanisms for boulder deposition on the southeast Australian coast. *Geomorphology*, 114, 42–54.
- Tomassetti, J. M., Arteaga, C., Navarro, I., Parra, L., Neogi, S., Taylor, S., Narváez, C., Torres, F., & Alcántara-Carrió, J. (2021). Sedimentological, geoarchaeological and historical evidences of the 881 AD Earthquake and Tsunami in the Western Mediterranean Sea (Estepona, Málaga). *The Science of Tsunami Hazards*, 40, 42–71.
- Vázquez, J. T., Ercilla, G., Alonso, B., Pelaez, J. P., Palomino, D., León, R., Bárcenas, P., Casas, D., Estrada, F., Fernández-Puga, M. C., Galindo-Zaldívar, J., Henares, J., Llorente, M., & Sánchez Guillamón, O. (2021). Triggering processes of tsunamis in the Alboran Sea and Gulf of Cádiz: A general review. In M. Álvarez Martí-Aguilar & F. Machuca Prieto (Eds.), *Historical Earthquakes and Tsunamis in the Iberian Peninsula—an Interdisciplinary Dialogue* (pp. 65–104). Springer Earth System Sciences.
- Vött, A., Brückner, H., May, M., Lang, F., Herd, R., & Brockmüller, S. (2008). Strong tsunami impact on the Bay of Aghios Nikolaos and its environs (NW Greece) during Classical-Hellenistic times. *Quaternary International*, 181, 105–122.
- Vött, A., Bruins, H. J., Gawehn, M., Goodman-Tchernov, B. N., De Martini, P. M., Kelletat, D., Mastronuzzi, G., Reicherter, K., Röbbke, B. R., Scheffers, A., Willershäuser, T., Avramidis, P., Bellanova, P., Costa, P. J. M., Finkler, C., Hadler, H., Koster, B., Lario, J., Reinhardt, E., ... Szczuciński, W. (2019). Publicity waves based on manipulated geoscientific data suggesting climatic trigger for majority of tsunami findings in the Mediterranean. *Zeitschrift Für Geomorphologie*, 62, 7–45.
- Weijermars, R. (1987). The Palomares brittle-ductile shear zone of southern Spain. *Journal of Structural Geology*, 9, 139–157.
- Whelan, F., & Kelletat, D. (2005). Boulder deposits on the southern Spanish Atlantic coast: Possible evidence for the 1755 AD Lisbon tsunami? *The Science of Tsunami Hazards*, 23, 22–38.
- Yamada, M., Fujino, S., & Goto, K. (2014). Deposition of sediments of diverse sizes by the 2011 Tohoku-oki tsunami at Miyako City, Japan. *Marine Geology*, 358, 67–78.
- Zazo, C., Goy, J. L., Dabrio, C. J., Lario, J., González-Delgado, A., Bardají, T., Hillaire-Marcel, C., Cabero, A., Ghaleb, B., Borja, F., Silva, P. G., Roquero, E., & Soler, V. (2013). Retracing the quaternary history of sea-level changes in the Spanish Mediterranean–Atlantic coasts: Geomorphological and sedimentological approach. *Geomorphology*, 196, 36–49.